CHARACTERIZATION AT DIFFERENT ASPECT RATIOS (RADIUS/LENGTH) OF A RADIO FREQUENCY INDUCTIVELY COUPLED PLASMA SOURCE

by

P. N. Wainman, M. A. Lieberman, A. J. Lichtenberg,
R. A. Stewart, and C. Lee

Memorandum No. UCB/ERL M94/56

20 July 1994

CHARACTERIZATION AT DIFFERENT ASPECT RATIOS (RADIUS/LENGTH) OF A RADIO FREQUENCY INDUCTIVELY COUPLED PLASMA SOURCE

by

P. N. Wainman, M. A. Lieberman, A. J. Lichtenberg,
R. A. Stewart, and C. Lee

Memorandum No. UCB/ERL M94/56

20 July 1994

ELECTRONICS RESEARCH LABORATORY

College of Engineering
University of California, Berkeley
94720

CHARACTERIZATION AT DIFFERENT ASPECT RATIOS (RADIUS/LENGTH) OF A RADIO FREQUENCY INDUCTIVELY COUPLED PLASMA SOURCE

by

P. N. Wainman, M. A. Lieberman, A. J. Lichtenberg,
R. A. Stewart, and C. Lee

Memorandum No. UCB/ERL M94/56

20 July 1994

ELECTRONICS RESEARCH LABORATORY

College of Engineering
University of California, Berkeley
94720

Characterization at Different Aspect Ratios (Radius/Length) of a Radio Frequency Inductively Coupled Plasma Source

P. N. Wainman, M. A. Lieberman, and A. J. Lichtenberg

Department of Electrical Engineering and Computer Sciences, University of California, Berkeley, CA 94720

R. A. Stewart and C. Lee

Department of Chemical Engineering, University of California, Berkeley, CA 94720

Ion densities, electron temperatures, plasma potentials, and absorbed powers are measured in a planar inductively coupled argon plasma source at different input powers, pressures, and aspect ratios (radius/length) and are compared to both a global (volume-averaged) model and a 2D fluid model. Qualitatively, the trends between the models and experiment are similar. Radial ion density profiles at different aspect ratios and pressures are also measured. An ion density peak off-axis is measured at a high aspect ratio and predicted by the 2D fluid model.

I. Introduction

The need for electronic devices with feature sizes as low as 0.25 μm has driven the design of plasma sources with capabilities beyond those offered by the conventional diode-type reactors. This is because such a small critical dimension requires high anisotropy, which in turn requires operation at lower pressures. With conventional reactors this requirement necessitates high powers to achieve sufficient throughput. However, since in the diode-type reactors the ion energy and flux are coupled together, this leads to very high ion bombarding energies which can cause damage.

To solve these problems, several sources have been introduced which can offer low pressure high density operation with decoupled ion energy and flux. One of the most promising sources is the planar RF inductively coupled plasma (ICP) source, which offers the additional advantages of simple design and good uniformity without external magnets. Typically, the ICP is run at pressures between 1 and 20 mTorr and powers from 200-1500 Watts, generating peak ion densities of 10^{11} - 10^{12} cm^{-3}.[1]

The ICP was first described in patents filed by Coultras and Keller of IBM Corporation[2] and by Ogle of Lam Research Corporation.[3] Since then, there have been several articles characterizing this source which are relevant to this study. Keller et al. have measured ion densities and etch rates,[4] Hopwood et al. have examined electromagnetic fields and ion density uniformity, plasma potential, and electron temperature,[1,5] and Mahoney et al. have described spatial profiles of electron density and energy and plasma potential.[6-8] In addition, Ra et al. have examined ion densities and etching of aluminum and photoresist[9] and Beale et al.[10] and O'Neill et al.[11] have used optical emission spectroscopy to characterize an argon discharge. To date, however, there has been only one reported study of ICP characterization at different aspect ratios[8] (which we define as R/L, the ratio of chamber radius R to height L). A better understanding of how plasma parameters are affected by the aspect ratio should assist in optimizing ICP reactor designs for process uniformity and control.

In this study we determine the electron temperature, ion density, and plasma potential in a

planar inductively coupled argon plasma source. The measurements are made using a cylindrical Langmuir probe at five reactor aspect ratios: R/L = 1, 1.5, 2, 3, and 4. All measurements are taken in the center of the discharge except for the radial density profiles. We also determine the actual rf power absorbed by the discharge for a given rf input power to the matching network that drives the ICP source. The organization of the paper is as follows. We first give an overview of the experimental apparatus and of the method used in the Langmuir probe measurements. We then discuss our results which are broken into three studies. First, we compare the measured electron temperatures for various aspect ratios, pressures, and powers to a global (volume-averaged) model[12] and to a 2D ICP fluid model[13] (described below). Next we compare ion densities with the models in the center of the discharge at different powers and pressures at the five aspect ratios, obtaining qualitative agreement. We also examine radial density profiles at the different aspect ratios in the axial center and compare them with the fluid model. Finally, we analyze the plasma potential at the five aspect ratios as a function of electron temperature and see trends similar to theory.

II. Experimental Apparatus and Method

A schematic diagram of the plasma source is shown in Figure 1. The plasma chamber is an aluminum cylinder with an inside diameter of 30 cm and a length of 1 meter. Moveable aluminum pistons are at both ends. An aluminum electrode, 27 cm in diameter, is mounted on one of these pistons. A 2.5 cm thick by 25 cm diameter quartz plate which separates our planar spiral induction coil from the plasma is mounted on the other piston. The 800 nH coil consists of three turns of copper strip, 0.06 cm wide by 1.9 cm thick, with 3 cm spacing between turns, which is placed 0.3 cm away from the quartz plate. For all measurements, the aluminum plasma chamber, pistons, and electrode are grounded. The chamber is pumped with a diffusion pump backed by a mechanical pump, giving a base pressure of about 4×10^{-6} Torr.

The source is powered at 13.56 MHz with a 1000 W Henry 1000D Radio Frequency Power Generator connected to an L-type capacitive matching network. The matching network provides a match with negligible reflected power for all the cases discussed in this article. A Bird Electronics Model 43 watt meter is placed between the generator and the matching network to measure the power absorbed in both the plasma and the matching network/power cable. In many of the recent studies, this has been the power value reported.[1,6-8] In order to determine the power actually absorbed in the plasma, we also measure the power deposited in the matching network/ power cable. This is done by setting the same current in the coil with no plasma as with a plasma and measuring the power absorbed by the system. The no-plasma condition was obtained by running the system at atmospheric pressure. Current measurements were made using a Pearson Model 411 current transformer. To insure that without a plasma we were not inducing significant image currents on the aluminum electrode which would skew our absorbed power measurements, we compared our power measurements with the same current settings at different aspect ratios. No significant difference was seen. Depending on the parameters, using this method, the power actually absorbed in the plasma ranges from only 4% (with capacitive coupling) to 45% (with inductive coupling) of the power absorbed in both the plasma and the matching network/power cable. Hereafter, the expression input power refers to the power deposited in both the matching

network/power cable and plasma, and the expression absorbed power refers to the power which is actually absorbed in the plasma.

Measurements of plasma parameters were made using a cylindrical Langmuir probe consisting of a tungsten wire 0.08 mm in diameter and 7.2 mm long. The probe tip is connected to a series of parallel LC elements within the probe shaft. These elements are chosen to resonate at 13.56 and 27.12 MHz, so that the probe tip will follow plasma potential oscillations. Measurements are taken in both the ion saturation and electron retardation portions of the *I-V* curve to determine ion density and electron temperature respectively. Since $r_{pr}/\lambda_D < 1$, where r_{pr} is the probe radius and λ_D is the electron Debye length, we use the orbital motion theory to determine the ion density:[14]

$$n_i = \frac{I_i}{e r_{pr} l_{pr} \sqrt{-8e\frac{(V_{pr} - V_{pl})}{m_i}}} \qquad (1)$$

where n_i is the ion density, m_i is the ion mass, I_i is the ion current, V_{pr} is the probe voltage, e is the (unsigned) electron charge, V_{pl} is the plasma potential, and l_{pr} is the probe length. In the ion saturation region where the probe current I_{pr} is virtually all ion current ($I_i \approx I_{pr}$), we can plot I_{pr}^2 vs. V_{pr} and fit to this a straight line $I_i^2 = AV_{pr} + B$. The slope A can then be substituted into Eq. (1) to determine n_i. Figures 2 and 3 illustrate this technique. In Figure 2, we show the probe data taken in both the ion saturation and electron retardation regions from one of our experimental runs. In this example, we estimate that the ion saturation regime extends from approximately V_{pr} = -40 V to V_{pr} = -5 V. In Figure 3, we isolate this region where we assume that the probe current is all ion current and plot I_{pr}^2 vs. V_{pr}. To this we fit a line as shown and determine the slope A.

To determine the electron temperature T_e, we need to determine the probe electron current $I_e = I_{pr} - I_i$ in the electron retardation region. To estimate the ion current I_i in this region, we extend the best fit line described above in the ion saturation region until it reaches $I_i = 0$ at which point we set the ion current to zero for all greater probe voltages. This best fit line represents the

square of the ion current so we simply take the square root to approximate I_i. Because the electron current to the probe is dependent upon the probe voltage through the Boltzmann factor $\exp[(V_{pr}-V_{pl})/T_e]$, we can determine T_e by calculating the slope of a line fitted to the graph of $\ln I_e$ vs. V_{pr}. The plasma potential, V_{pl}, is then found using the relation:[15]

$$V_{pl} - V_f = \frac{T_e}{2} + \frac{T_e}{2}\ln\left(\frac{m_i}{2\pi \cdot m_e}\right) \qquad (2)$$

where V_f is the measured floating potential of the probe ($I_{pr} \equiv 0$), T_e is the electron temperature in volts, and m_e is the electron mass. The first term on the right-hand side of Eq. (2) is the initial energy of an ion entering the sheath, and the second term is the energy gained by the ion as it traverses the sheath. For argon, the right-hand side of Eq. (2) reduces to approximately 5.2 T_e.

The measurements are compared to both a global (volume-averaged) model and a 2D fluid model. The global model, as described more completely in the comparisons, assumes a uniform density except at the sheath edge. A detailed description of the model is given in reference 12. The fluid model includes equations for electron and (Ar+) ion continuity, ion momentum balance, electron energy balance, and poisson's equation, in (r,z) cylindrical geometry. Electron flux is assumed to consist of drift and diffusion, and local, time-averaged collisional heating from the rf inductive electric field is included in the electron energy equation. The inductive heating is calculated self-consistently using the local plasma conductivity, coil currents and voltages, by solving a subset of Maxwell's equations for the time-averaged rf electric field in the plasma. A more detailed description of the fluid and power coupling models using are given in references 13 and 17, respectively.

III. Results

When taking measurements we noticed a change in the plasma as we went from low input power to high input power. At low input power, the plasma is dim and the percent absorbed power and consequently the ion density are low. As we increase the power, a short transition region is

entered where the plasma becomes much brighter, the match changes, and the percentage of power that is absorbed increases greatly. Where this transition region occurs depends on the pressure and the aspect ratio. We assume that at low power before this transition region, capacitive coupling dominates and that after this transition region, inductive coupling dominates. On the graphs discussed below, the points representing those in the capacitive regime are filled in. These points are not taken into consideration when discussing comparisons to theory and computer models.

We measured the electron temperature at five aspect ratios, R/L = 1, 1.5, 2, 3, and 4, in the center of the discharge with the following parameters: (1) at an input power of 300 W with pressures of 2, 5, and 20 mTorr and (2) at 5 mTorr with input powers of 100, 200, and 300 W. To present the data in a unified form, we plot the results as a function of $n_g d_{eff}$ where n_g is the neutral gas density and d_{eff} is the effective plasma size. Lieberman and Gottscho showed, within a global (volume-averaged) high-density argon source model, that T_e is a function of $n_g d_{eff}$ only.[15] The effective plasma size, d_{eff}, is defined as[15]

$$d_{eff} = \frac{RL}{2\,(Rh_L + Lh_R)} \tag{3}$$

which comes from equating the total volume ionization to the surface particle loss

$$K_{iz} n_g n_0 \pi R^2 L = n_0 u_B\,(2\pi R^2 h_L + 2\pi R L h_R) \tag{4}$$

and solving to obtain

$$\frac{K_{iz}}{u_B} = \frac{1}{n_g d_{eff}} \quad . \tag{5}$$

We define h_L as

$$h_L \equiv \frac{n_{sL}}{n_0} \approx 0.86\,(3 + \frac{L}{2\lambda_i})^{-1/2} \tag{6}$$

and h_R as

$$h_R \equiv \frac{n_{sR}}{n_0} \approx 0.80\,(4 + \frac{R}{\lambda_i})^{-1/2}. \qquad (7)$$

Here λ_i is the ion-neutral mean free path, n_{sL} is the ion density at the axial sheath edges $z = 0$ and $z = L$, n_{sR} is the ion density at the radial sheath edge $r = R$, K_{iz} is the electron-neutral ionization rate constant, $u_B = (eT_e/m_i)^{1/2}$ is the Bohm velocity, and n_0 is the average center ion density assuming the flat density profile as shown in Figure 4. In Figure 5, we compare the experimental data with the results from both the global and fluid models, finding excellent correspondence over the entire range of aspect ratios, pressures, and powers. Note that the data from the fluid model is at various aspect ratios. The trends are the same as those reported in previous studies of argon discharges; the electron temperature is fairly independent of power and decreases with increasing pressure.[1,7]

In Figure 6, we show ion density versus $P_{abs}d_{eff}/V\varepsilon_L u_B e$, a universal parameter, as described below. Here P_{abs} is the power absorbed by the plasma, d_{eff} is as defined above, $V = \pi R^2 L$ is the volume of the plasma chamber, and ε_L is the total energy lost per ion lost from the system. Measurements of the ion density are taken in the center of the discharge for the five aspect ratios shown. Two of the data points for each aspect ratio are at pressures of 2 and 20 mTorr with the other points at 5 mTorr. Absorbed powers range from 2 to 170 Watts.

From the global model, assuming the flat density profile in Figure 4, the average ion density should be equal to $P_{abs}d_{eff}/V\varepsilon_L u_B e$. This is derived as follows.[15] The overall source power balance equation is defined as

$$P_{abs} = e n_s u_B A \varepsilon_L \qquad (8)$$

where n_s is the ion density at the plasma-sheath edge, and $A = 2\pi(R^2 + RL)$ is the area for particle

loss. Introducing the effective loss area through $n_s A = n_0 A_{eff}$ and using Eq. (8), we obtain

$$n_i = n_0 = \frac{P_{abs} d_{eff}}{V \varepsilon_L u_B e} \tag{9}$$

where $A_{eff} = V/d_{eff}$ and n_0 is the average ion density. The solid line drawn shows where the values should lie, according to this model. Values for ε_L and u_B for the experiment and fluid model data points were generated using the global model.[12] Note that the trend of the measured values follows those of both the models and those reported in other studies,[1,4,6,7,9] in that the ion density, for each aspect ratio, depends linearly on power.

However, as shown in Figure 6, significant quantitative differences exist among the three sets of data (experiment, global model, and fluid model). One possible reason for the lower global model ion density values is that the model derives an average ion density and assumes a flat profile in the center. But, in reality, our radial profile measurements (see below) suggest that the ion density profile is not flat in the center but follows more of a J_0 Bessel function radially (and presumably a sine function axially). To try to account for this profile and using the fact that the average of a sine function over half a cycle is $2/\pi$ and that the average of a J_0 Bessel function is $\approx$ 0.43, we can change Eq. (9) to:

$$n_0 = 3.64 \frac{P_{abs} d_{eff}}{V \varepsilon_L u_B e} \tag{10}$$

where n_0 now represents the peak ion density. This expression is plotted as the dotted line in Figure 6.

Radial measurements of ion density, normalized to the center density, are shown in Figures 7 (a), (b), and (c) at 2, 5, and 20 mTorr respectively. These are compared with radial profiles predicted from the fluid model. The measurements and simulations are all in the mid-plane of the chamber. As expected, as pressure and aspect ratio increase, the profiles become more peaked in the center. The fluid model also follows this trend, although the change in profiles with

aspect ratio is not as marked. As the pressure increases, the fluid model seems to follow the experimental data more closely. Note that we observe an off-axis ion density peak with our experimental data for an aspect ratio of 4 at pressures of 5 and 20 mT. This is also shown by the fluid model for the same aspect ratio at 20 mT. An aspect ratio of 4 corresponds to a radius of 15.1 cm and a length of 3.8 cm -- a short squat reactor. Such an off-axis density peak can be explained by examining the inductive electric field. As discussed by Hopwood et al.[5] and Mahoney et al.,[7] the inductive electric field peaks at approximately half the radius of the coil, and goes to zero in the center of the discharge. The absorbed power is proportional to the square of the electric field and therefore also peaks at ~ *R/2*. At most pressures and aspect ratios, because the heated electrons diffuse rapidly, the ion density is peaked in the center. At high pressures and aspect ratios, however, thermal conductivity is inhibited and axial losses increase, thus creating a peak in density off-axis.[17]

In Figure 8, we show plasma potential V_{pl} versus the electron temperature T_e for our five aspect ratios. Measurements are taken at the center of the discharge. Two of the data points at each aspect ratio are at pressures of 2 and 20 mTorr, with the rest at various powers at 5 mTorr. If best-fit lines were drawn for each aspect ratio, the slopes of these lines would be 5.7, 5.5, 5.0, 6.0, and 7.0 for aspect ratios of 1, 1.5, 2, 3, and 4 respectively. These slopes, with the exception of that for the aspect ratio of 4, are reasonably consistent with the theory given in Eq. (2), which says that the slope should be 5.2. The large values of plasma potential are due to the large measured values of floating potential in our reactor which ranged from 9 to 18 V.

IV. Conclusion and Discussion

Measurements of ion density, electron temperature, absorbed power, and plasma potential have been performed for five aspect ratios at various pressures and input powers in the center of an inductive discharge. Comparisons have been made between these measurements and a global (volume-averaged) model and a 2D fluid model. Qualitative agreement was found between the models and measurements. It was found that one should measure the power which is actually

absorbed by the plasma as this can be much different from the power put into the plasma + matching network/transmission cable.

At the axial center at three pressures, radial ion density scans were performed for five aspect ratios and compared with a fluid model. The ion density uniformity was seen to change significantly with aspect ratio. An off-axis ion density peak was observed experimentally and predicted by the fluid model at high pressure and large aspect ratio.

It is important to note that Eq. (10), which is the modified expression used by the global model to determine center ion density, is not generally correct since the ion density profile changes significantly with aspect ratio and with pressure as seen in Figures 7 (a), (b), and (c). We therefore do not expect our experimental data to line up with the model curves in Figure 6, but rather we show them to compare trends. Another possible reason for the discrepancy between the models and experiment in Figure 6 is that using orbital motion limit (OML) theory to determine ion density in the ion saturation region is not quantitatively accurate. Godyak et al.[16] have showed that by using OML, one measures ion densities that are 2-3 times larger than the actual values.

V. Acknowledgments

This work was supported in part by NSF Grant ECS-9217500, DOE Grant DE-FG03-87ER13727, and LLNL Grant W-7405-ENG-48.

References

[1] J. Hopwood, C. R. Guarnieri, S. J. Whitehair, and J. J. Cuomo, *J. Vac. Sci. Technol.* A **11**, 152 (1993).

[2] D. K. Coultas, and J. H. Keller, European Patent, Publication No. 0 379 828 A2 (8 January 1990).

[3] J. S. Ogle, U.S. Patent No. 4,948,458 (14 August 1990).

[4] J. H. Keller, J. C. Forster, M. S. Barnes, *J. Vac. Sci Technol.* A **11**, 2487 (1993).

[5] J. Hopwood, C. R. Guarnieri, S. J. Whitehair, and J. J. Cuomo, *J. Vac. Sci. Technol.* A **11**, 147 (1993).

[6] L. J. Mahoney, A. E. Wendt, E. Barriros, C. J. Richards, and J. L. Shohet, *J. Appl. Phys.* **76**, (1994), to be published.

[7] L. J. Mahoney, G. Li, A. E. Wendt, J. L. Shohet, D. Beal, and H. Yu, AVS 39th National Symposium, Chicago, Illinois, November 9, 1992 (unpublished).

[8] L. J. Mahoney, A. E. Wendt, and J. L. Shohet, International Conference on Plasma Science, Sante Fe, New Mexico, June 6, 1994 (unpublished).

[9] Y. Ra, S. G. Bradley, and C. H. Chen, submitted for publication.

[10] D. F. Beale, A. E. Wendt, and L. J. Mahoney, *J. Vac. Sci. Technol.* A, (1994), to be published.

[11] J. A. O'Neill, M. S. Barnes, and J. H. Keller, *J. Appl. Phys.* **73** 1621 (1993).

[12] C. Lee and M. A. Lieberman, submitted for publication.

[13] R. A. Stewart, P. Vitello, D. B. Graves, E. F. Jaeger, and L. A. Berry, submitted for publication.

[14] J. G. Laframboise, Inst. for Aero. Stud., Univ. of Toronto, Rep. No. 100 (1966), Sect. 14 and Fig. 40.

[15] M. A. Lieberman and R. A. Gottscho, *Physics of Thin Films*, ed. by M. Francombe and J. Vossen, Academic Press, Vol. 18, 1994.

[16] V. A. Godyak, R. B. Piejak, and B. M. Alexandrovich, *J. Appl. Phys.* **73**, 3657 (1993).

[17] R. A. Stewart, P. Vitello, and D. B. Graves, *J. Vac. Sci. Technol.* B **12**, 478 (1994).

Figure Captions

Figure 1. Schematic of ICP source: rf power (1), matching network (2), induction coil (3), quartz plate (4), Langmuir probe (5), vacuum chamber (6), gas inlet (7), chamber sides (8), end plate (9).

Figure 2. Probe current versus probe voltage. This typical scan taken at 5 mT, $R/L = 1$, and P_{abs} = 43 W.

Figure 3. The probe current squared versus probe voltage in the ion saturation region for the scan in Figure 2.

Figure 4. The ion density profile assumed by the global model.

Figure 5. Electron temperature T_e vs. $n_g d_{eff}$. Solid points correspond to those in the capacitive regime.

Figure 6. Ion density n_0 vs. $P_{abs} d_{eff}/V \varepsilon_L u_B e$. Experiment and fluid model values correspond to center densities. Solid line represents values predicted by the global model with the profiles shown in Figure 4. Dotted line represents the corrected center ion density obtained for an ion density profile which is a sine in z and a J_0 Bessel function in r. Solid points correspond to those in the capacitive regime.

Figures 7 (a), (b), and (c). Ion density (normalized to the center density) vs. radius at a pressure of (a) 2 mT, (b) 5 mT, and (c) 20 mT. The lines shown represent fluid model results.

Figure 8. Plasma potential vs. electron temperature T_e. Solid points represent those in the capacitive regime.

Figure 1

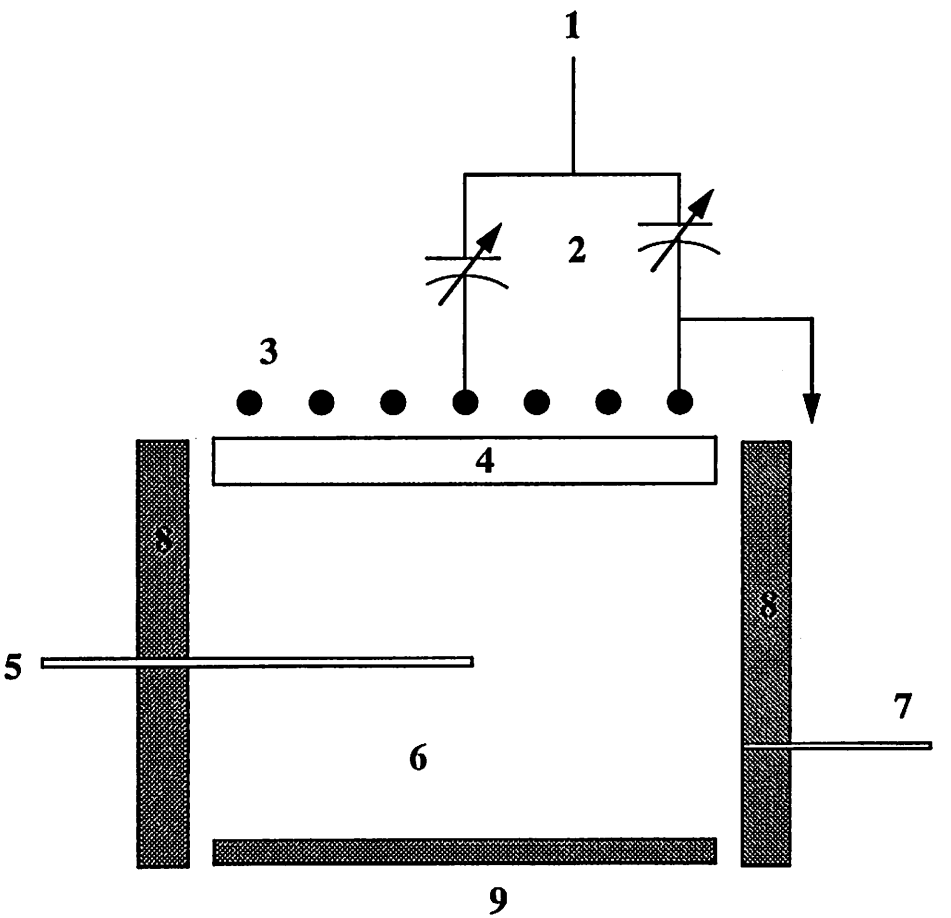

Figure 2

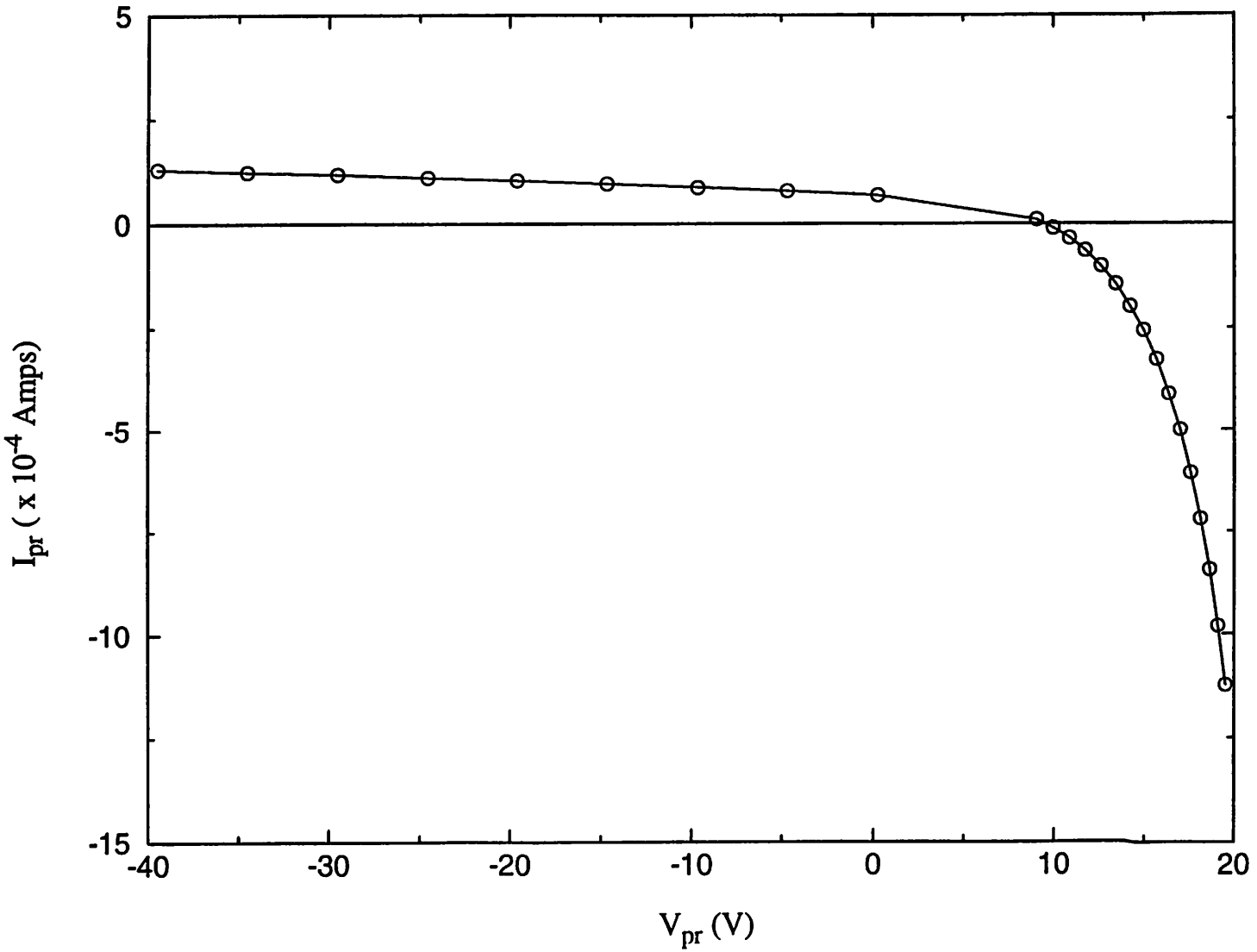

Figure 3

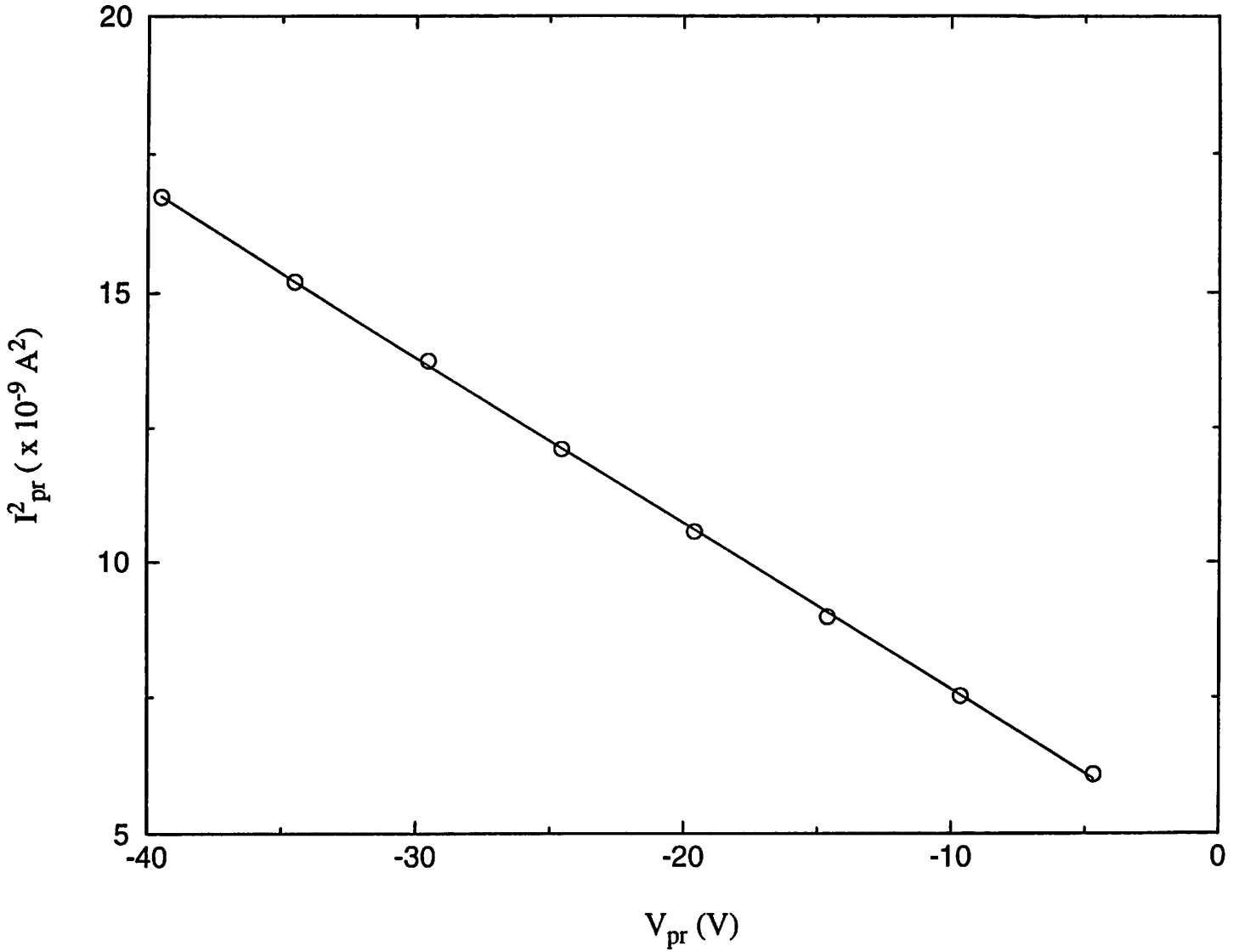

Figure 4

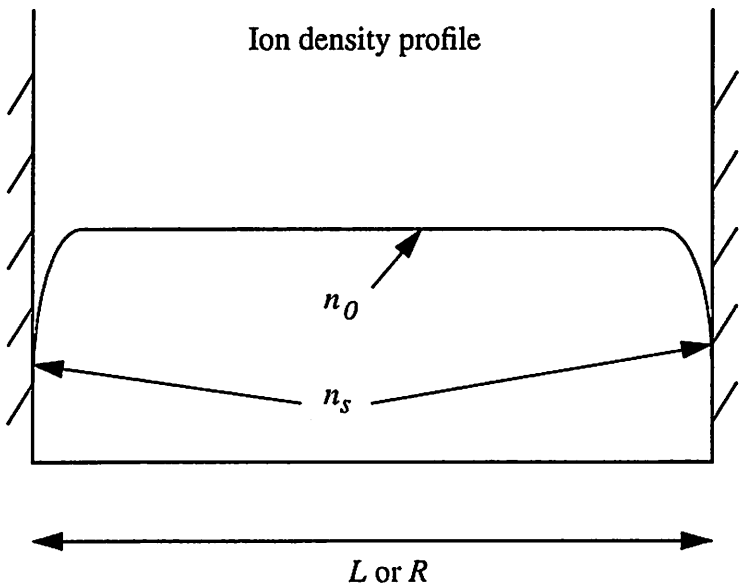

Figure 5

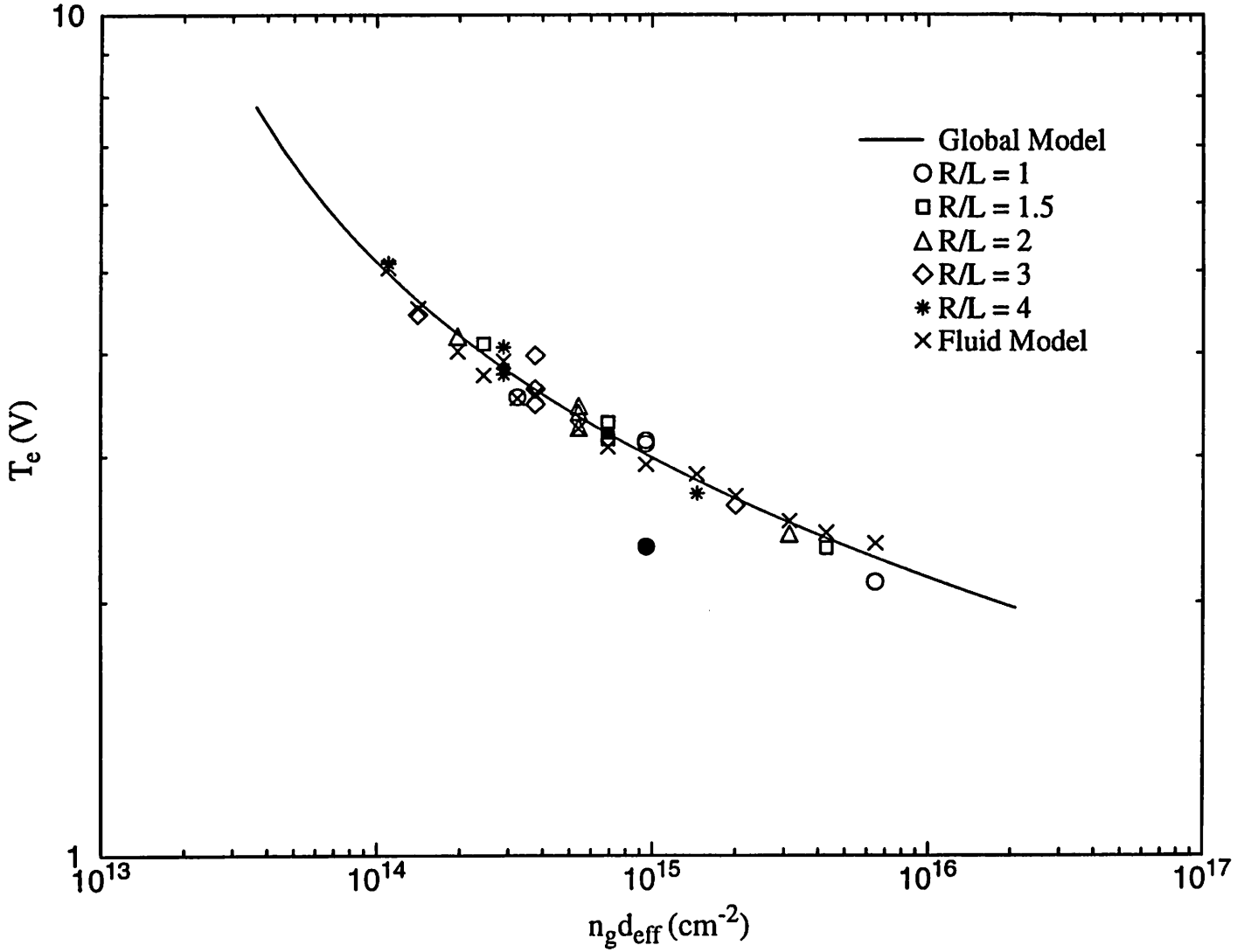
10
1
10^{13}
10^{14}
10^{15}
10^{16}
10^{17}
T_e (V)
$n_g d_{eff}$ (cm^{-2})
Global Model
R/L = 1
R/L = 1.5
R/L = 2
R/L = 3
R/L = 4
Fluid Model

Figure 6

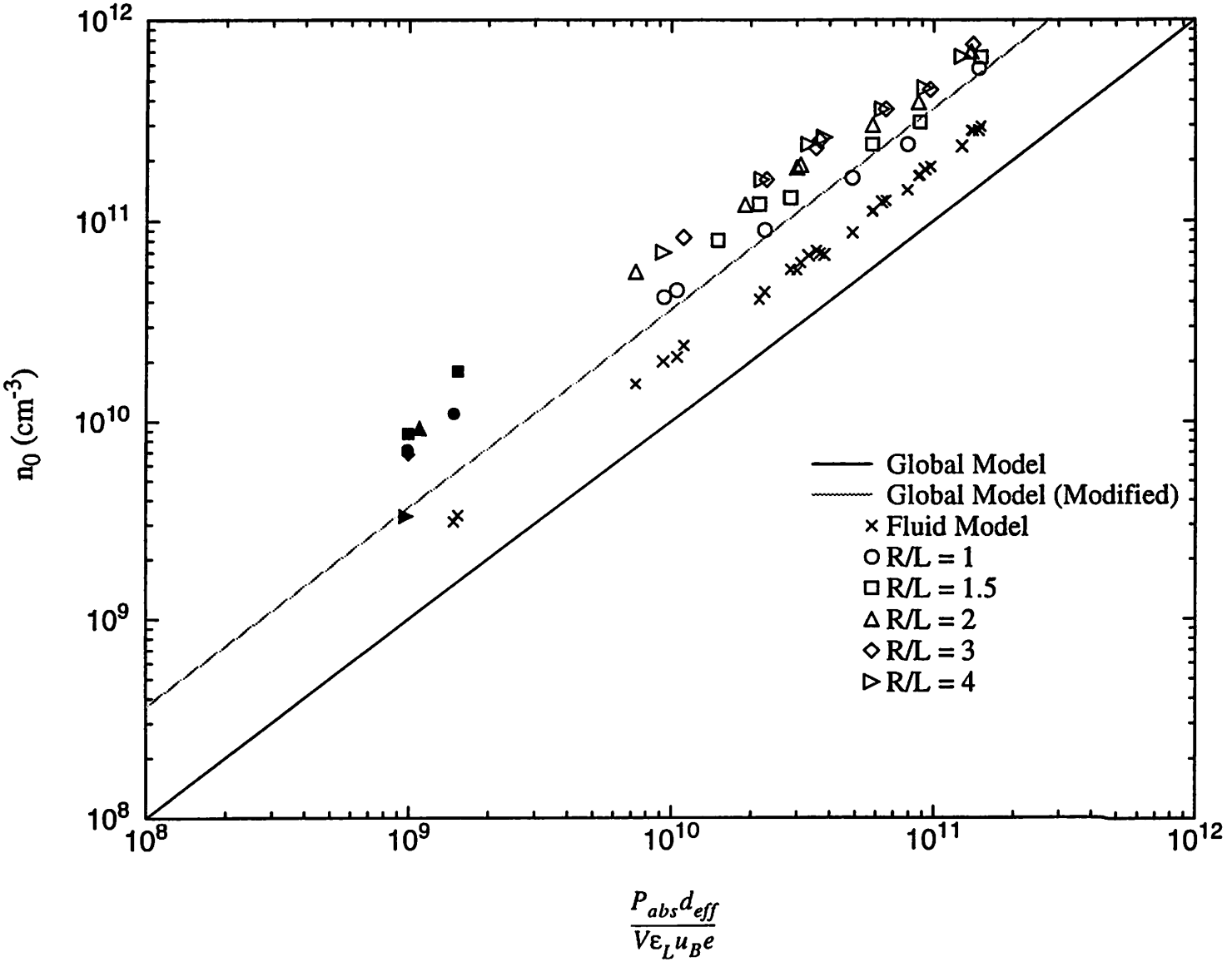
10^{12}
10^{11}
10^{10}
10^{9}
10^{8}
n_0 (cm^{-3})
10^{8}
10^{9}
10^{10}
10^{11}
10^{12}
$\frac{P_{abs}d_{eff}}{V\varepsilon_L u_B e}$
Global Model
Global Model (Modified)
× Fluid Model
○ R/L = 1
□ R/L = 1.5
△ R/L = 2
◇ R/L = 3
▷ R/L = 4

Figure 7a

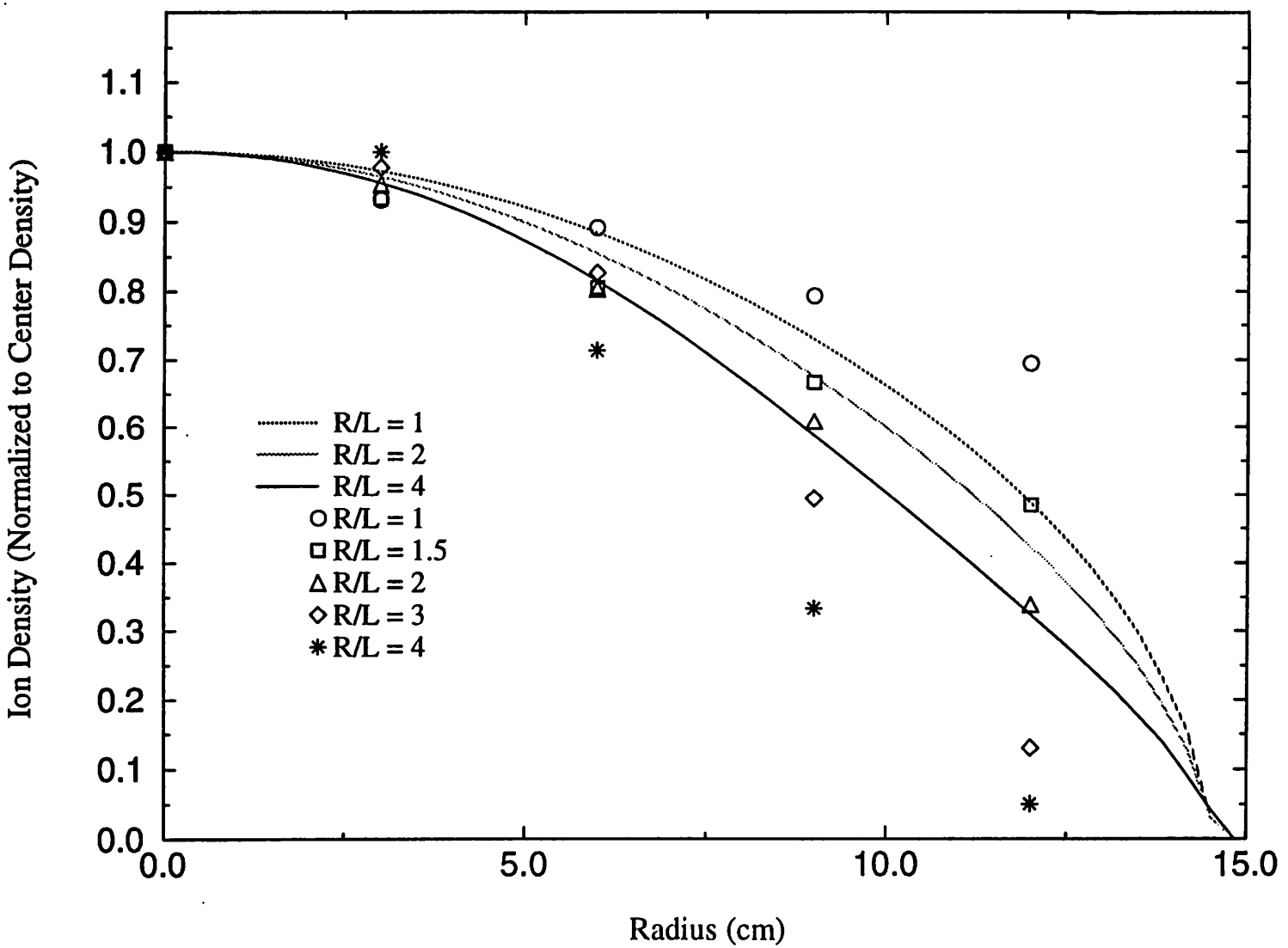
Ion Density (Normalized to Center Density)
1.1
1.0
0.9
0.8
0.7
0.6
0.5
0.4
0.3
0.2
0.1
0.0
0.0
5.0
10.0
15.0
Radius (cm)
R/L = 1
R/L = 2
R/L = 4
R/L = 1
R/L = 1.5
R/L = 2
R/L = 3
R/L = 4

Figure 7b

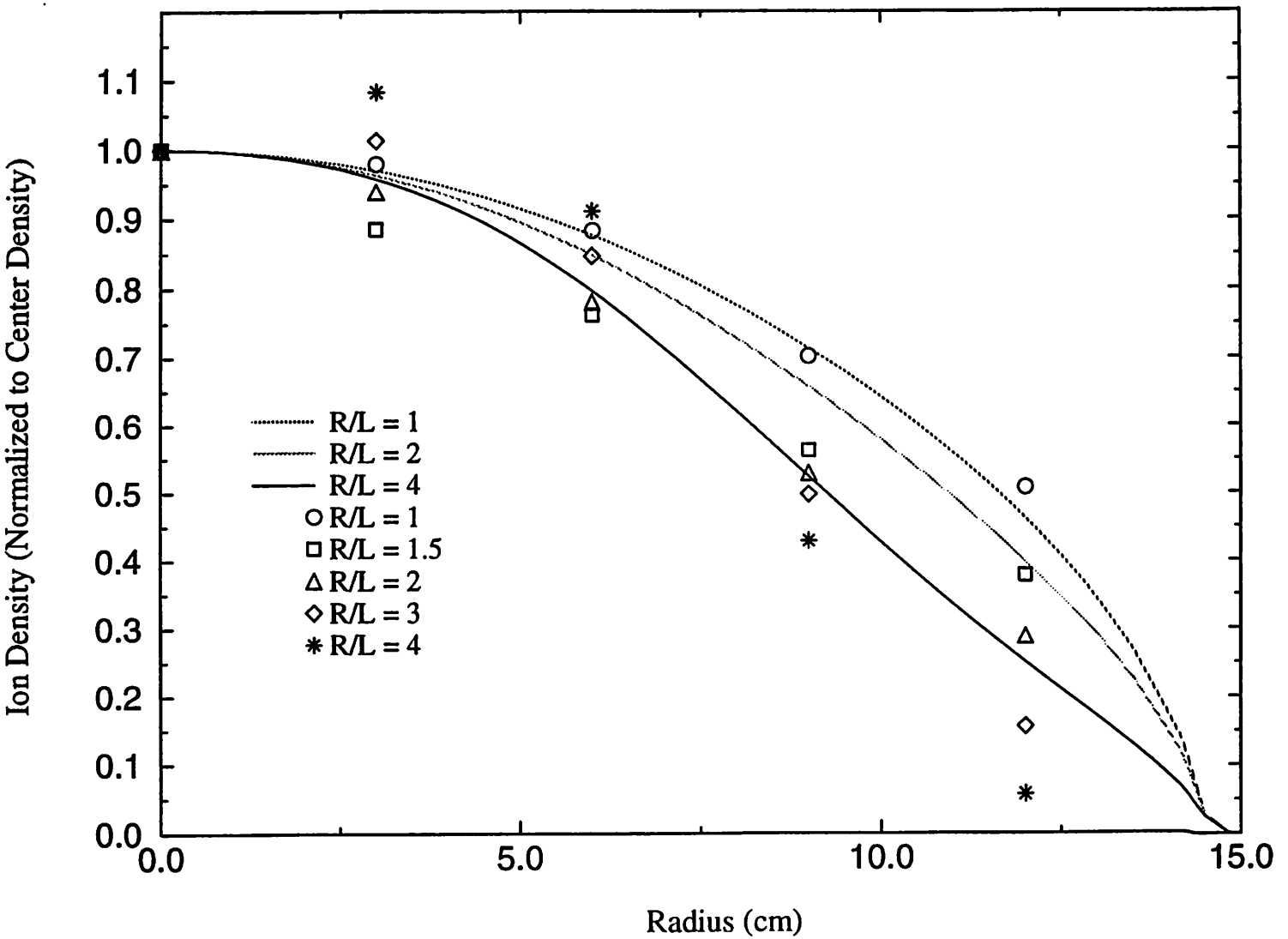
Ion Density (Normalized to Center Density)
1.1
1.0
0.9
0.8
0.7
0.6
0.5
0.4
0.3
0.2
0.1
0.0
0.0
5.0
10.0
15.0
Radius (cm)
R/L = 1
R/L = 2
R/L = 4
R/L = 1
R/L = 1.5
R/L = 2
R/L = 3
R/L = 4

Figure 7c

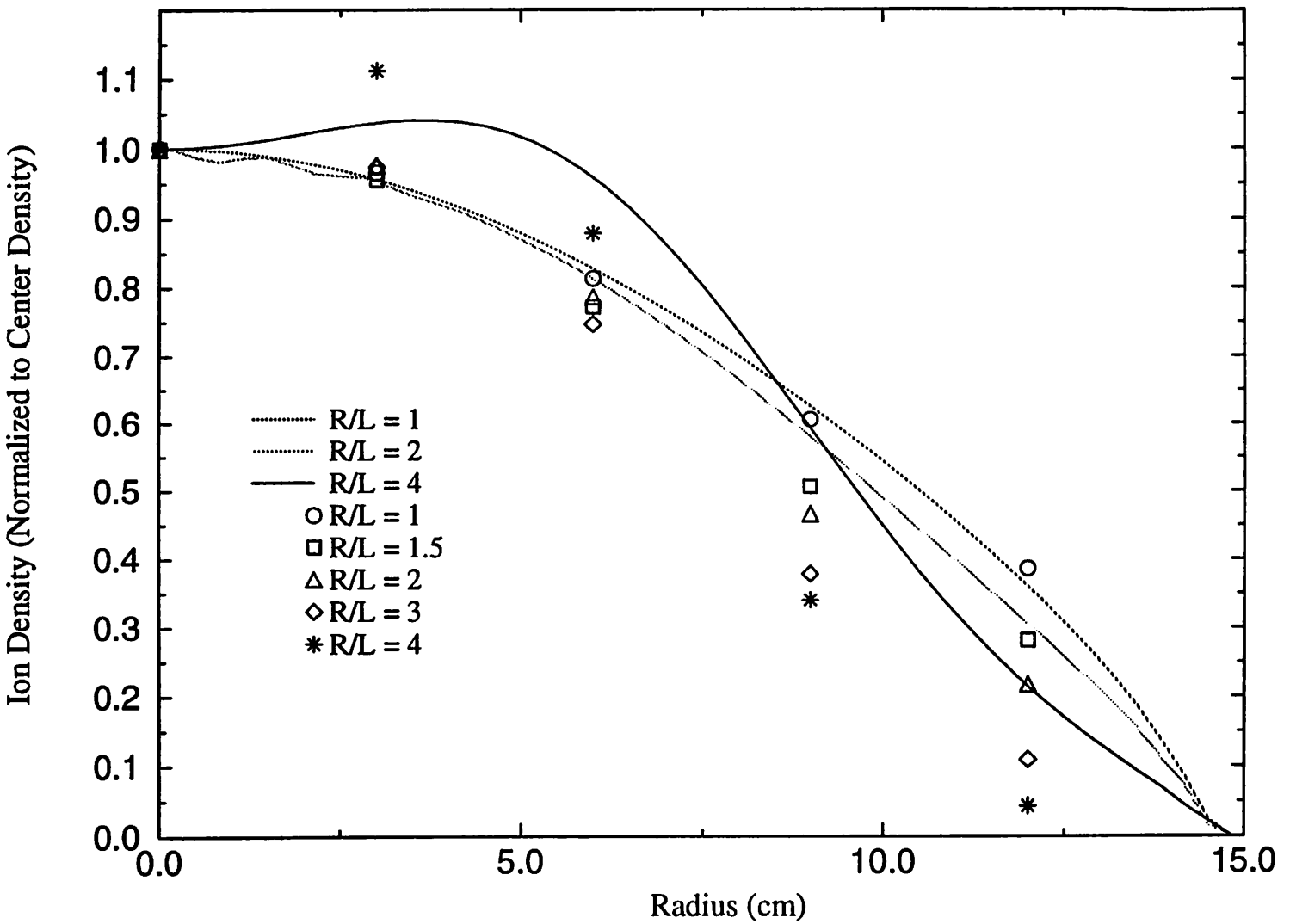
Ion Density (Normalized to Center Density)
Radius (cm)
0.0
0.1
0.2
0.3
0.4
0.5
0.6
0.7
0.8
0.9
1.0
1.1
0.0
5.0
10.0
15.0
R/L = 1
R/L = 2
R/L = 4
R/L = 1
R/L = 1.5
R/L = 2
R/L = 3
R/L = 4

Figure 8